International Journal of Nanomedicine

Dovepress

open access to scientific and medical research

Open Access Full Text Article

ORIGINAL RESEARCH

Combined Dextran-Graft-Polyacrylamide/Zinc Oxide Nanocarrier for Effective Anticancer Therapy in vitro

Vasyl Chumachenko[1], Pavlo Virych[1], Guochao Nie[2], Petro Virych[3], Oleg Yeshchenko[4], Pavlo Khort[4], Anton Tkachenko[5], Volodymyr Prokopiuk[5,6], Nataliia Lukianova[3], Taras Zadvornyi[3], Michel Rawiso[7], Liyao Ding[2], Nataliya Kutsevol[1,7]

[1]Chemistry Department, Taras Shevchenko National University of Kyiv, Kyiv, Ukraine; [2]Guangxi Universities Key Laboratory of Complex System Optimization and Big Data Processing, Yulin Normal University, Yulin, People's Republic of China; [3]Laboratory of Mechanisms of Drug Resistance, R.E. Kavetsky Institute for Experimental Pathology, Oncology and Radiobiology, Kyiv, Ukraine; [4]Physics Department, Taras Shevchenko National University of Kyiv, Kyiv, Ukraine; [5]Research Institute of Experimental and Clinical Medicine, Kharkiv National Medical University, Kharkiv, Ukraine; [6]Department of Cryobiochemistry, Institute for Problems of Cryobiology and Cryomedicine of the National Academy of Sciences of Ukraine, Kharkiv, Ukraine; [7]Institut Charles Sadron, Strasbourg, France

Correspondence: Guochao Nie, Guangxi Universities Key Laboratory of Complex System Optimization and Big Data Processing, Yulin Normal University, Yulin, 537000, People's Republic of China, Tel +86-17377071871, Email bccu518@163.com; Pavlo Virych, Chemistry Department, Taras Shevchenko National University of Kyiv, 60 Volodymyrska str., Kyiv, 01601, Ukraine, Tel +380-631172137, Email pavlo.virych@knu.ua

Introduction: Cancer chemotherapy faces two major challenges – high toxicity of active substances and tumor resistance to drugs. Low toxic nanocarriers in combination with anticancer agents can significantly increase the effectiveness of therapy. Modern advances in nanotechnology make it easy to create materials with the necessary physical and chemical properties.

Methods: Two hybrid nanosystems of dextran-polyacrylamide/ zinc oxide nanoparticles (D-PAA/ZnO NPs) were synthesized in aqueous solution with zinc sulphate (D-PAA/ZnO NPs (SO_4^{2-})) and zinc acetate (D-PAA/ZnO NPs (-OAc)). The light absorption, fluorescence, dynamic light scattering and transmission electron microscopy for nanocomposite characterization were used. MTT, neutral red uptake and scratch assays were selected as fibroblasts cytotoxicity assays. Cytotoxicity was tested in vitro for normal fibroblasts, MAEC, prostate (LNCaP, PC-3, DU-145) and breast (MDA-MB-231, MCF-7) cancer cells lines. Immunocytochemical methods were used for detection of Ki-67, p53, Bcl-2, Bax, e-cadherin, N-cadherin and CD44 expression. Acridine orange was used to detect morphological changes in cells.

Results: The radius of ZnO NPs (SO_4^{2-}) was 1.5 nm and ZnO NPs (-OAc) was 2 nm. The nanosystems were low-toxic to fibroblasts, MAEC. Cells in the last stages of apoptosis with the formation of apoptotic bodies were detected for all investigated cancer cell lines. Proapoptotic proteins expression in cancer cells indicates an apoptotic death. Increased expression of E-cadherin and N-cadherin was registered for cancer cells line LNCaP, PC-3, DU-145 and MCF-7 after 48 h incubation with D-PAA/ZnO NPs (SO_4^{2-}).

Conclusion: The nanosystems were low-toxic to fibroblasts, MAEC. The D-PAA/ZnO NPs nanosystem synthesized using zinc sulphate demonstrates high cytotoxicity due to destruction of various types of cancer cells in vitro and potentially increases adhesion between cells. Thus, our findings indicate the selective cytotoxicity of D-PAA/ZnO NPs against cancer cells and can be potentially used for cancer treatment.

Keywords: zinc oxide nanoparticles, polymer nanocarrier, drug delivery, cytotoxicity, prostate cancer, breast cancer

Introduction

Nanotechnology in medicine is becoming a promising approach in antitumor therapy, which includes photodynamic therapy, chemotherapy, radiation therapy, etc. The development of new nanotechnology-based anticancer agents is now drawing considerable attention. An increasing number of studies have demonstrated that low concentrations of metal-containing nanoparticles (NPs), including metal oxide NPs, can damage cancer cells, while their larger micrometer-sized

Received: 27 April 2023
Accepted: 13 August 2023
Published: 28 August 2023

counterparts are comparatively non-toxic.[1–4] However, NPs can be toxic to both tumor and normal cells due to their non-selective effects. To overcome these adverse effects, a multidisciplinary approach is needed in the study of nanosystems.[5]

Fundamental studies of participation of microelements in physiologically important processes allow understanding their importance in maintaining homeostasis. Over a long period of time, little attention has been paid to zinc. This microelement is involved in immune responses, cell cycle regulation, cell differentiation and proliferation, DNA and RNA synthesis and repair, enzyme activity regulation, intercellular and intracellular signaling, and membrane stabilization, among other functions.[6–8]

Zinc oxide nanoparticles (ZnO NPs) are regarded as a potent agent for anticancer therapy since they are cytotoxic against tumor cells. This cytotoxicity can be attributed to their ability to modify the activity of zinc-dependent proteins. Zinc impacts the initiation and inhibition of apoptosis due to alterations in both intracellular and postcellular concentrations.[9–11] ZnO NPs possess various properties, including electrostatic charge and surface chemistry activity, that can be beneficial for anticancer treatment due to their antitumor cytotoxic actions.[12] The electrostatic charge of NPs is crucial, as electrostatic interactions between positively charged NPs and target cells play a significant role in cellular adhesion and uptake.[13] The shape and morphology of NPs also present important parameters for their biomedical applications.[14] An advantage of applying ZnO NPs in cancer treatment is their preferential cytotoxicity against cancer cells in vitro.[15] This selectivity towards cancer cells may be enhanced by engineering NPs to minimize detrimental effects on normal cells, a phenomenon observed at high concentrations of ZnO NPs with sizes between 4–20 nm.[16] An increasing body of evidence suggests that certain types of cancer tumors are associated with a decrease in pH.[17,76] When pH decreases, ZnO NPs release zinc ions, which locally increase their concentration.[18]

Hypoxia and high glycolytic activity are common traits of solid tumors. These metabolic changes result in the excretion of lactate and protons into the intercellular space. Combined with an underdeveloped vasculature, these conditions reduce the environmental pH to 6.5–6.9, while the intracellular pH remains neutral or slightly alkaline. This situation creates an acid gradient, which is not typical for normal tissues and prevents weak bases from penetrating tumor cells.[19,20] Furthermore, there's a decrease in apoptotic potential, genetic changes, and activation of p-glycoprotein. P-glycoprotein acts as a drug transporter and contributes to the multidrug resistance of cancer cells.[21] It has been reported that ZnO NPs can kill cancer cells through the induction of oxidative stress.[22] The mechanisms of ZnO NPs cytotoxicity are not entirely understood, but the generation of reactive oxygen species (ROS) seems to play a major role in promoting cell death.[23,24]

The development of nanotechnologies allows for the creation of systems that deliver necessary biologically active components into tissues. This approach enhances the effectiveness of drugs and reduces their toxicity.[25] The creation of drug delivery systems considers certain physiological characteristics of tumors. One such feature is the high hydrostatic pressure of the interstitial fluid, which directs flow outward, causing the removal of therapeutic agents from tumor cells.[26] The heterogeneity of tumors serves as an additional barrier, restricting the diffusion of a drug throughout the tumor. The effectiveness of chemotherapeutic agent carriers greatly depends on the physicochemical properties of NPs, including their surface structure, charge, size, etc.[27] Polymer nanocarriers can be designed to be biocompatible, serving simultaneously as a matrix for the synthesis of metallic nanoparticles (Me NPs) of specific sizes while preventing their aggregation.[28,29] The macromolecular parameters and chemical nature of the polymer affect the biodistribution, pharmacokinetics, and therapeutic properties of antitumor agents.[30–32] Moreover, some polymers can confer extended half-lives to the drug delivery system and enable prolonged drug desorption. The macromolecular structure of polymers determines their drug capacity and interaction with target cells.[33] Combining ZnO NPs with such carriers expands the potential anticancer properties of nanocomposites against tumors of varying aggressiveness and resistance to chemotherapy.[21]

The aim of our research was to synthesize stable aqueous solutions of zinc oxide NPs from two precursors, zinc acetate and zinc sulphate, within a branched dextran-polyacrylamide polymer matrix using the precipitation method. We studied the physical characteristics of the obtained nanosystems through optical methods, dynamic light scattering, and transmission electron microscopy. Additionally, we aimed to investigate the cytotoxicity of ZnO NPs-containing nanosystems on prostate and breast cancer cell lines with distinct physiological features of intracellular zinc regulation. Finally, we intended to determine the cytotoxicity of these nanosystems on normal cells.

Materials and Methods

All chemicals utilized in the synthesis of hybrid nanosystems were purchased from Merck (Munich, Germany) and were used without further purification unless explicitly stated otherwise.

Dextran-Graft-Polyacrylamide Macromolecular Parameters

The branched star-shape copolymer Dextran-graft-Polyacrylamide (D-PAA) was used as a nanocarrier and matrix for ZnO NPs in synthesis. The D-PAA synthesis and peculiarities of polymer structure have been reported in detail previously.[33] The branched structure of D-PAA provides high stability of nanosystems prepared in these copolymer.[27,28,30] In the present research, we used a D-PAA copolymer with Dextran core (Mw=$20{\cdot}10^5$ g·mol^{-1}) and average number of polyacrylamide arms equal to 10, molecular characteristics of this polymer were: Mw = $9.5{\cdot}10^5$ g·mol^{-1}, and Mw/Mn = 1.62.

Synthesis of Dextran-Graft-Polyacrylamide/ZnO Nanoparticles

Two samples with different counter ions, D-PAA/ZnO NPs(-OAc) and D-PAA/ZnO NPs(SO_4^{2-}), were prepared using the precipitation method. Initially, 1 mL of a $ZnSO_4$ solution (0.1 mol·mL^{-1}) or 1 mL of a $Zn(OAc)_2$ solution (0.1 mol·mL^{-1}) was added to 5 mL of an aqueous D-PAA solution (10^3 g·mL^{-1}). After 20 minutes, 2 mL of a sodium hydroxide solution (0.1 mol·mL^{-1}) was added dropwise to the vigorously stirred D-PAA/$ZnSO_4$ or D-PAA/$Zn(OAc)_2$ mixtures. These solutions were then continuously stirred at 50°C for 24 hours to yield D-PAA/ZnO NPs(-OAc) or D-PAA/ZnO NPs(SO_4^{2-}).

Optical Characterization

The light absorption spectra were recorded using a Cary 60 UV-VIS spectrophotometer (Agilent, Santa Clara, California, USA). The fluorescence (FL) spectra were measured with a Shimadzu RF-6000 spectrofluorophotometer (Shimadzu, Kyoto, Japan), using a wavelength of 250 nm for FL excitation. The solution samples were placed in a polished quartz cell with dimensions of 1cm×1cm×4cm. Both the absorption and FL spectra were measured at room temperature.

Dynamic Light Scattering

Dynamic light scattering (DLS) measurements were performed using the NanoBrook Omni particle size analyzer (Brookhaven Instruments, Holtsville, New York, USA), equipped with a 532 nm diode laser. The concentrations of D-PAA, D-PAA/ZnO NPs(-OAc), and D-PAA/ZnO NPs(SO_4^{2-}) solutions were adjusted by adding water to reach a diluted regime (where D-PAA concentration was 10^{-5} g·mL^{-1}) in which the hydrodynamic radius of the D-PAA macromolecule does not depend on the concentration. The light scattered was detected at a backscattering angle of 173°. The samples were maintained at 25°C for 5 minutes to reach equilibrium. At least 10 correlation curves for each sample were processed by an algorithm based on singular value decomposition (SVD) implemented in the Python 3.8 programming language in order to evaluate the particle size distribution (PSD).

Transmission Electronic Microscopy

The observations of the ZnO NPs were carried out using a JEM 1000 (JEOL, Tokyo, Japan). For sample preparation, copper grids with a plain carbon film (Elmo, Cordouan Technologies, Bordeaux, France) were used. A 5 µL drop of the sample was deposited on the grid and allowed to adsorb for 1 minute; then, any excess solution was removed using a piece of filter paper. Image processing and size measurements were carried out using ImageJ 1.4 software.

Cytotoxicity Assays Performed on Fibroblasts

Rat embryo skin served as the source of fibroblasts for the preparation of primary cell cultures, which were prepared using trypsinization.[26,34] Freshly isolated skin fragments were treated with 0.25% trypsin-EDTA (BioWest, Nuaille, France) for 60 minutes at 37°C, mixed using a magnetic stirrer. The investigations was carried out in accordance with the legislation in force in Ukraine, international ethical requirements and was not violate ethical norms in science and standards for biomedical research (Committee on Ethics and Bioethics of the Kharkiv National Medical University,

protocol #9 of November 3, 2021). After enzyme inactivation and filtration, the cells were washed with DMEM (BioWest) and 10% fetal bovine serum (FBS, BioWest), then seeded in 25 cm^2 culture flasks (SPL, Pyeongtaek, Republic of Korea) and harvested using 0.25% trypsin-EDTA. The study utilized cells that had undergone 3–4 passages. These cells were incubated in 96-well plates with DMEM medium and 5% FBS for 24 hours at 37°C, with the addition of ZnO NPs using a two-fold dilution method at concentrations ranging from 0.756 mM to 12.3 mM. Each concentration of hybrid nanocomposites was represented by eight samples.

MTT, neutral red uptake, and scratch assays were selected to measure cytotoxicity. Additionally, the impact of nanocomposites on the fibroblast monolayer was analyzed. Following the protocol of the MTT assay, after incubating cells with nanocomposites in 96-well plates (SPL) containing 1×10^4 cells per well at 37°C and under 5% CO_2, the medium was discarded. Subsequently, 0.1 mL of culture medium and 15 µL of MTT were added for further incubation under 5% CO_2 at 37°C for 180 minutes. The medium was supplemented with 100 µL of DMSO and SDS and incubated for an additional hour at 37°C. Quantitative analysis involved measuring absorbance at 570 nm using a StatFax 303+ analyzer (Awareness Technology, Palm City, Florida, USA). Numerical values were presented in optical density (OD) units.

For the neutral red uptake assay, fibroblasts were incubated with nanocomposites as previously described, then exposed to 0.1 mL of culture media containing 0.003% neutral red dye for 3 hours under 5% carbon dioxide. After extracting the neutral red dye with 0.1 mL of a solution containing 50% ethanol and 3% acetic acid, the absorbance at 570 nm was measured using a StatFax 303+ analyzer (Awareness Technology). Numerical values were presented in OD units.

The scratch assay was employed to evaluate how nanocomposites alter cell motility. Fibroblasts, seeded in 24-well plates (SPL) at a density of 15×10^4 cells per well, were incubated with nanocomposites as previously detailed. Prior to this, a scratch of a fixed width was created in the monolayer using a pipette tip. Following incubation, images of the monolayers were captured using a Delta Optical NIB 100 inverted microscope (Delta Optical, Warsaw, Poland) equipped with a Sigeta MCMOS 3100 3.1MP camera. The width of the scratch was analyzed in five regions for each sample. Numerical values were presented in millimeters.

In vitro Cytotoxicity for Cancer Cells

The studies were carried out on prostate cancer cells DU-145, PC-3, LNCaP, breast cancer cells MDA-MB-231, MCF-7, and normal cells MAEC. Reference cultures were obtained from the cell bank of the R.E. Kavetsky Institute of Experimental Pathology, Oncology, and Radiobiology, National Academy of Science of Ukraine. Cells were maintained in plastic flasks (SPL) in DMEM (L0103, Biowest) supplemented with 10% fetal calf serum (Biowest) and 40 µg/mL gentamicin (Merck). The cells were incubated at 37°C in a humidified atmosphere containing 5% CO_2. D-PAA/ZnO NPs were added to the incubation solution through double dilution within the concentration range of 0.05–0.000781 M and left for 48 hours. The medium was replaced with fresh DMEM containing various concentrations of ZnO NPs. The number of living cells was calculated photometrically after staining with crystal violet. The incubation medium was removed, and 50 µL of a 0.5% solution of crystalline violet in 70% methanol was added to each well and left to stain for 10 minutes. The excess dye was washed off three times with water. The results were measured using a Labsystems Multiskan PLUS spectrophotometer (Vantaa, Finland) at 540 nm. The relative change in the cell population was calculated as follows:

$$CD = \left(1 - \frac{D_{sample}}{D_{control}}\right) * 100\%$$

where CD is the relative change in cell number, expressed as a percentage; D_{sample} is the absorbance at 540 nm of an experimental sample; and $D_{control}$ is the absorbance at 540 nm of a control sample. The obtained dose-response results were processed in accordance with the Hill equation.[34] The half-maximal effective concentration (EC50) was calculated for future immunocytochemical investigations. Each experiment was repeated three times.

Acridine orange (Merck) was used to detect morphological changes in cancer cells. A 1 mg/mL stock solution was prepared in 0.9% sodium chloride. Cancer cells were incubated for 24 hours with the half-maximal effective concentration (EC50) of D-PAA/ZnO NPs(SO_4^{2-}). A working solution of acridine orange was prepared in saline solution, resulting in a final dye concentration of 0.002 mg/mL. Cells were stained for 1 minute and then washed for 1 minute. Fluorescence

studies were carried out using an Olympus BX53 microscope (Tokyo, Japan) with an XCite Series 120 Q luminescence block and an Olympus DP72 camera. All samples were examined under the same conditions: exposure of 10 ms, a red-to-green color ratio of 2:1 when recording luminescence, excitation with a blue light filter, and emission of green and red light. At least 10 separate fields of view were photographed for each sample. Each experiment was repeated five times.

The expression of p53, Ki-67, Bcl-2, Bax, E-cadherin, N-cadherin, and CD44 was investigated using anti-p53, anti-Ki-67, anti-Bcl-2, anti-Bax, anti-E-cadherin, anti-N-cadherin, and anti-CD44 antibodies, respectively (all from Merck). These antibodies were diluted in blocking buffer. Cells were fixed in a 1:1 methanol to acetone mixture at −20 °C for 120 minutes. After washing with phosphate-buffered saline (PBS), the cells were incubated with the aforementioned antibodies for 1 hour. The Ultra-Vision LP detection system (Thermo Scientific, Waltham, Massachusetts, USA) was used to detect bound antibodies. Following another round of washing, the immune response was visualized using the DAB Quanto system (Thermo Scientific). Protein expression was assessed using the H-score method, which is described as follows:

$$S = 0 \cdot N_0(\%) + 1 \cdot N_1(\%) + 2 \cdot N_2(\%) + 3 \cdot N_3(\%)$$

where S is the H-score index, N_0 is the number unstained cells, N_1, N_2, N_3 are the numbers of cells with low, medium or high levels of marker expression, respectively.[35] The difference in protein expression was calculated according to the equation:

$$D, \% = \left(1 - \frac{S_{sample}}{S_{control}}\right) * 100\%$$

Where D, % is a difference in protein expression, %; S_{sample} is an H-score index for sample cells; S_{sample} is an H-score index for control cells.

Statistical Analysis

Statistical data processing was carried out using the one-way ANOVA Scheffe test (M±SD; $p<0.05$). Kruskal–Wallis and Dunn's tests were used to compare the cell cytotoxicity results using Graph Pad Prism 5.0 application (GraphPad, Boston, Massachusetts, USA). The difference was statistically significant at $p<0.05$.

Results and Discussion

Dynamic Light Scattering (DLS) was employed to determine the size of nanoparticles. This method measures the Brownian motion of nanoparticles and calculates their average size and the homogeneity of their size distribution.[36]

The size characteristics of the synthesized nanosystems were obtained using DLS, as depicted in Figure 1. The Particle Size Distribution (PSD) for the bare D-PAA polymer in solution indicated an average hydrodynamic radius (RH) of 38 nm (Figure 1, blue line). For both types of D-PAA/ZnO NPs nanosystems, those containing ZnO NPs(SO_4^{2-}) or ZnO NPs(-OAc), three size fractions were observed in the PSD derived from DLS.

The first PSD peak indicates the presence of subnanometer NPs with sizes of 0.6 and 0.3 nm for the acetate and sulfate precursors, respectively. This likely signifies that the RH derived from DLS is significantly underestimated, particularly for D-PAA/ZnO NPs(SO_4^{2-}). This underestimation for such small particles, coupled with the high scattering angle of $\theta = 173°$, results in the breaking of the limit $qR \ll 1$, where R is the particle size and q is the scattering vector, defined as $q = 4\pi/\lambda \sin\theta$. This limit is particularly crucial for particles with possible internal dynamics,[37] which is certainly the case for our system, as it includes polymer chains.

The second peak of PSD, located at 7 nm and 10 nm for D-PAA/ZnO NPs(SO_4^{2-}) and D-PAA/ZnO NPs(-OAc) respectively, corresponds to the ZnO NPs. The radii of the ZnO NPs obtained are in reasonable agreement with radii derived from absorption data, which will be discussed further. As with the first peak, the RH value is shifted towards larger sizes.

The third PSD peak, with RH > 240 nm, indicates an aggregation process, since free D-PAA macromolecules consist of considerably smaller particles. It's likely that the formation of zinc oxide NPs triggered the aggregation process in both D-PAA/ZnO NPs(-OAc) and D-PAA/ZnO NPs(SO_4^{2-}) nanosystems.

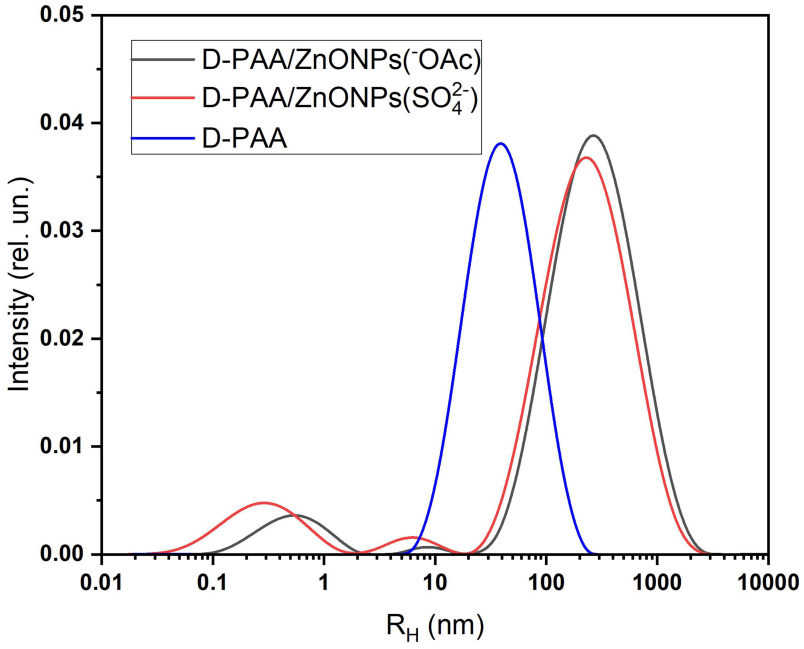

Figure 1 Hydrodynamic radius (R_H) of dextran-polyacrylamide/ZnO NPs from zinc acetate (D-PAA/ZnO NPs(-OAc)), zinc sulphate (D-PAA/ZnO NPs(SO_4^{2-})) and bare D-PAA.

The branched copolymer D-PAA stabilizes the NPs and prevents their aggregation. As a result, the synthesized nanosystems included smaller ZnO NPs were much smaller compared to NPs produced by applying other methods.[21] For instance, ZnO NPs obtained through green synthesis methods typically have diameters around 100 nm,[38,39] while sol-gel methods produce NPs ranging from 30 to 100 nm,[40–42] and co-precipitation methods yield NPs varying from 50 to 140 nm.[43,44] Many of these nanosystems included even large aggregates with size up to 200 nm.

In summary, our observations indicate that, for all three main size modes observed in the PSD, larger scatterers were observed for D-PAA/ZnO NPs(-OAc) compared to D-PAA/ZnO NPs(SO_4^{2-}).

Bulk ZnO is characterized by a wide direct band gap (3.4 eV) and a large exciton binding energy (60 meV), making it suitable for UV optical applications.[45] Moreover, due to the quantum confinement effect, the absorption and fluorescence spectra of ZnO NPs exhibit a blue shift compared to those of bulk ZnO. Respectively, ZnO NPs are characterized by high optical absorption in the UV region, ranging from 400 nm to 280 nm, depending on the size of the NPs.[46,47] The absorption and fluorescence spectra of ZnO NPs in solution can be utilized to determine their size based on the wavelengths of the respective spectral peaks.

Figure 2a and b depict the absorption and fluorescence spectra of ZnO NPs in D-PAA/ZnO NPs(-OAc) and D-PAA/ZnO NPs(SO_4^{2-}) respectively. It is evident that the absorption spectra of both samples exhibit clear exciton absorption peaks centered at 354 nm (corresponding to an energy of 3.5054 eV) for D-PAA/ZnO NPs(-OAc) and 349 nm (corresponding to an energy of 3.5544 eV) for D-PAA/ZnO NPs(SO_4^{2-}).

The exciton peaks were extracted from the absorption spectrum by fitting the spectra with basic Lorentzian peaks, as shown in Figure 2a as dotted lines. Both peaks exhibit a blue shift relative to the corresponding peak in bulk ZnO (3.3 eV), with a shift of 0.20 eV for D-PAA/ZnO NPs(-OAc) and 0.25 eV for D-PAA/ZnO NPs(SO_4^{2-}) nanosystems, respectively. These observed shifts can be attributed to the quantum confinement effect, well-known for semiconductor NPs. Based on the obtained blue shift values and considering the reference data[46] on the size dependence of the exciton absorption peak wavelength for ZnO NPs, the estimated radius of ZnO NPs in our samples is 2 nm for D-PAA/ZnO NPs (-OAc) and 1.5 nm for D-PAA/ZnO NPs(SO_4^{2-}) samples. Notably, the spectroscopically estimated sizes of ZnO NPs agree well with those obtained from the DLS data, especially considering the limited accuracy of DLS for small particles such as ZnO NPs.

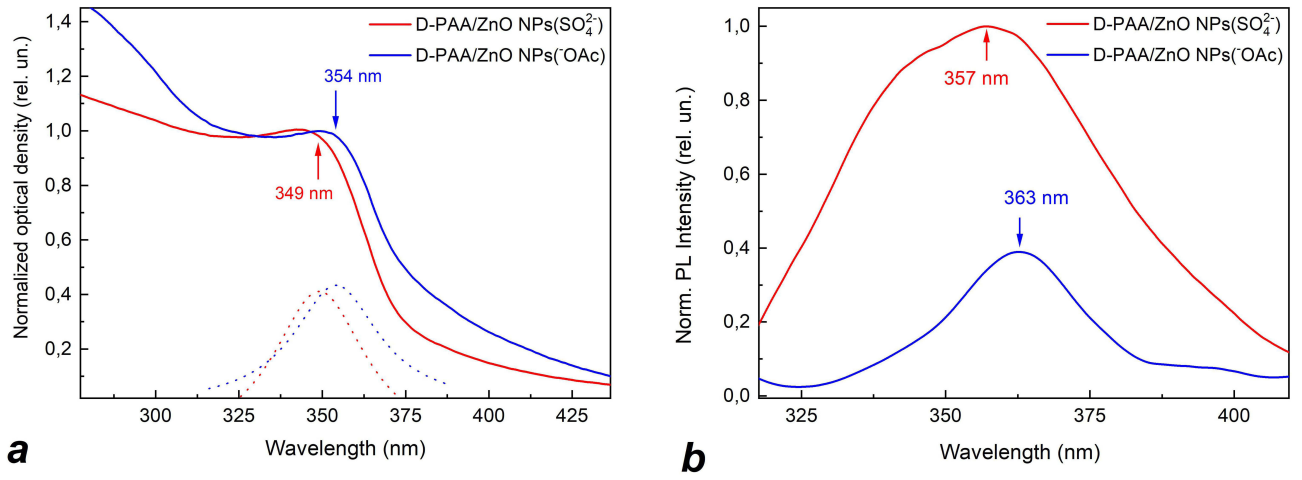

Figure 2 Normalized absorption (**a**) and fluorescence (**b**) spectra of ZnO NPs in water solution of dextran-polyacrylamide/ZnO NPs from zinc sulphate (D-PAA/ZnO NPs(SO_4^{2-})) – red line, zinc acetate (D-PAA/ZnO NPs(-OAc)) – blue line. The dotted lines in part (**a**) present the exciton absorption peaks extracted from the total spectra. The spectra were measured at room temperature.

The ZnO NPs in the studied colloidal samples exhibit fluorescence with maxima at 363 nm for D-PAA/ZnO NPs (-OAc) and 357 nm for D-PAA/ZnO NPs(SO_4^{2-}) samples. Similar to the absorption peaks, the fluorescence (FL) peaks of ZnO NPs in the samples are blue-shifted relative to the FL peak of exciton in bulk ZnO due to the quantum confinement effect. Additionally, it can be observed that the FL peaks have a red Stokes shift from the respective absorption peaks, namely 9 nm for D-PAA/ZnO NPs(-OAc) and 8 nm for D-PAA/ZnO NPs(SO_4^{2-}). This relatively small Stokes shift suggests a weak electron-phonon interaction in ZnO NPs. Furthermore, it is noteworthy that there is a significantly more intense fluorescence of ZnO NPs in the D-PAA/ZnO NPs(SO_4^{2}-) nanosystem compared to the D-PAA/ZnO NPs(-OAc) nanosystem. This could be attributed to two possible reasons. First, it may be due to the quantum effect of increasing the probability of radiative exciton transitions with a decrease in NP size. Second, it could be explained by a stronger aggregation process in D-PAA/ZnO NPs(-OAc), which could quench the FL.

The size distributions obtained from TEM images consistently showed a mean radius value of 1.0±0.5 nm (Figure 3). However, it is important to note that the absence of particles in some TEM images makes it challenging to directly compare and evaluate differences between samples, primarily due to the significant degradation of the samples under the

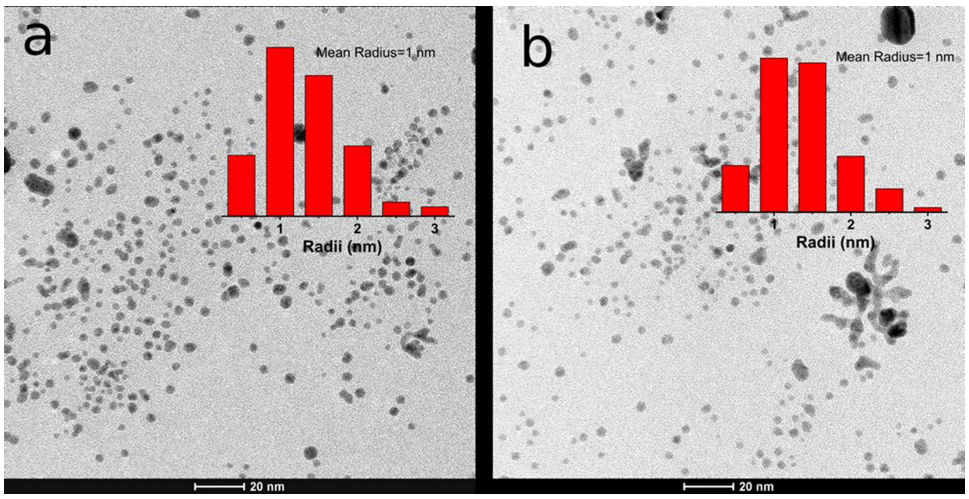

Figure 3 Transmission electron microscopy images and radii distributions of dextran-polyacrylamide/ZnO NPs from zinc sulphate (D-PAA/ZnO NPs(SO_4^{2-}) (**a**), and zinc acetate (D-PAA/ZnO NPs (-OAc) (**b**).

electron beam. Nevertheless, the TEM images do reveal the presence of particle aggregates with sizes of approximately 10–20 nm, which are also observable through the DLS method.

In general, the analysis of TEM images supports the conclusions regarding the size and size distribution derived from other measurement methods, providing further confirmation of the consistency in the observed particle characteristics.

Thus, proceeding from DLS and FL data, one can conclude that D-PAA/ZnO NPs(SO_4^{2-}) nanosystem seems to be more suitable for biomedical applications than D-PAA/ZnO NPs(-OAc) due to a smaller size of ZnO NPs and weaker aggregation.

The selectivity of anticancer drugs has a great importance. Zinc oxide NPs have shown promising evidence of inducing cancer cell death while having minimal negative effects on normal cells.[48–50] In our study, we investigated the sensitivity of fibroblasts to D-PAA/ZnO NPs(-OAc) and D-PAA/ZnO NPs(SO_4^{2-}). Microscopic examination revealed that D-PAA/ZnO NPs(-OAc) did not cause any noticeable changes in the fibroblast monolayer even at the highest concentrations. The number of cells, monolayer confluence, and adhesion remained unaffected (Figure 4).

The ability of ZnO NPs to penetrate the cell membrane, interact with proteins and DNA, and disrupt their functions has been established in numerous studies. ZnO NPs induce the production of reactive oxygen species (ROS), leading to oxidative stress, damage of the endoplasmic reticulum, and subsequent autophagy.[51,52]

Cell viability assays demonstrated that the survival of cells exposed to D-PAA/ZnO NPs(-OAc) was not compromised (Figure 5). The scratch assays indicated normal mobility of fibroblasts. In contrast, D-PAA/ZnO NPs(SO_4^{2-}) had a more pronounced impact on fibroblasts. At the highest concentration used, D-PAA/ZnO NPs(SO_4^{2-}) caused visible changes in the fibroblast monolayer, including a reduction of the cells number and diminished confluence (Figure 4). The MTT assay showed a reduction in cell viability, but this result was not supported by the neutral red uptake assay (Figure 5). Importantly, D-PAA/ZnO NPs(SO_4^{2-}) had a noticeable effect on the mobility of fibroblasts.

They statistically significantly reduced the functional activity of dermal fibroblasts at the concentrations of over 3.07 mM (Figures 6 and 7).

Our findings suggest that D-PAA/ZnO NPs(-OAc) exhibits lower toxicity against fibroblasts compared to D-PAA/ZnO NPs(SO_4^{2-}). This finding aligns with our hypothesis regarding the higher biomedical potential of the D-PAA/ZnO

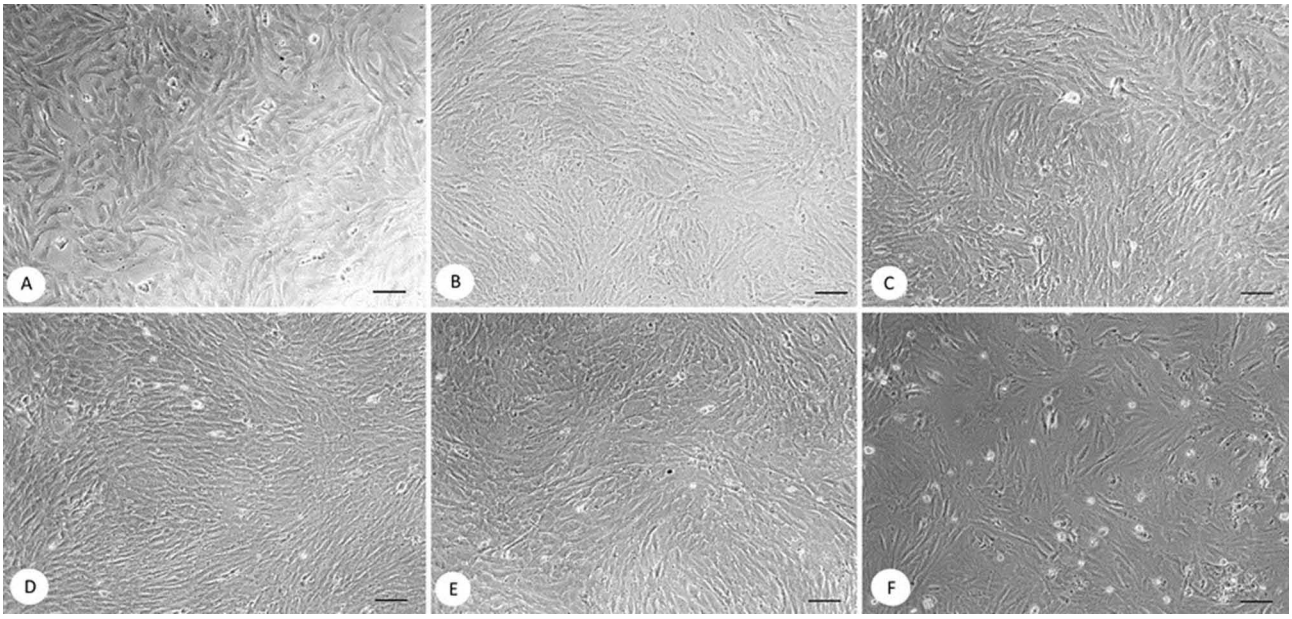

Figure 4 Microscopy of fibroblast monolayers exposed to hybrid nanocomposites: (**A**) intact cells before incubation (day 0); (**B**) fibroblast non-exposed to nanocomposites (day 1); (**C**) dermal fibroblasts exposed to 1.53 mM dextran-polyacrylamide/ZnO NPs from zinc acetate (D-PAA/ZnO NPs(-OAc)) nanocomposite; (**D**) cells treated with 12.3 mM D-PAA/ZnO NPs(-OAc) nanocomposite; (**E**) fibroblast monolayer incubated with 1.53 mM dextran-polyacrylamide/ZnO NPs from zinc sulphate (D-PAA/ZnO NPs(SO_4^{2-})) nanocomposite; (**F**) cells exposed to 12.3 mM D-PAA/ZnO NPs(SO_4^{2-}) nanocomposite. Scale bar: 100 µm. D-PAA/ZnO NPs(SO_4^{2-}) nanocomposite at the concentration of 12.3 mM altered the cell morphology and monolayer confluence.

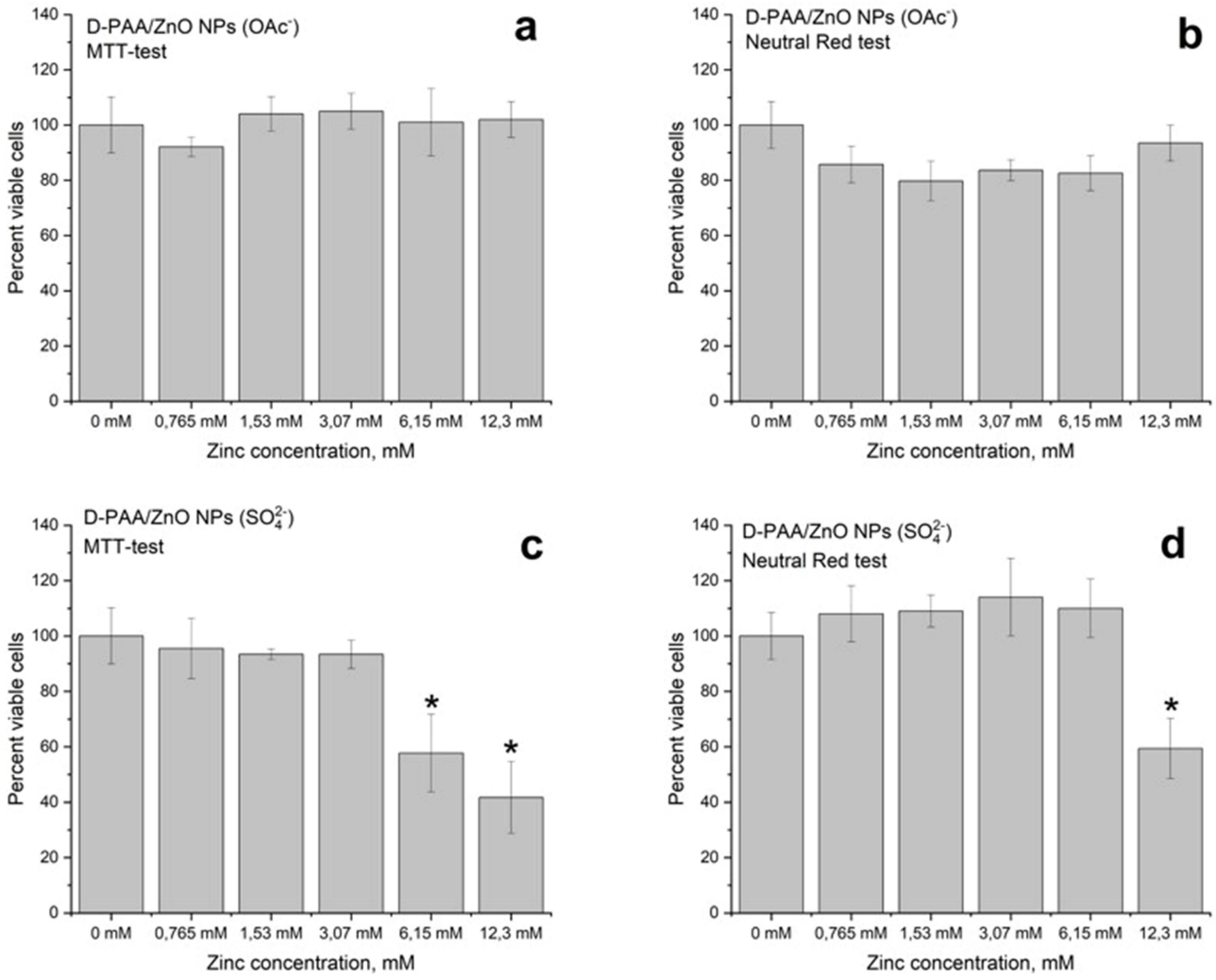

Figure 5 Results of cell cytotoxicity MTT (**a** and **c**) and neutral red (**b** and **d**) assays are used to assess the effects dextran-polyacrylamide/ZnO NPs from zinc acetate (D-PAA/ZnO NPs(-OAc)) and zinc sulphate (D-PAA/ZnO NPs(SO_4^{2-})) on fibroblast cultures (median, *p<0.05).

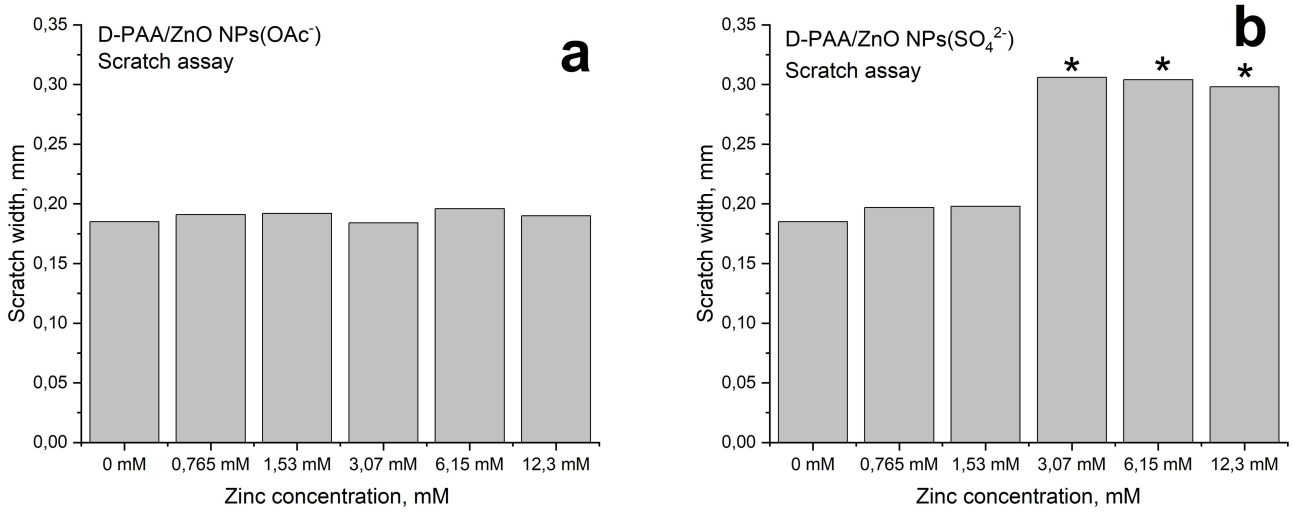

Figure 6 Fibroblasts migration in presence dextran-polyacrylamide/ZnO NPs from zinc acetate (D-PAA/ZnO NPs(-OAc)) (**a**) and zinc sulphate (D-PAA/ZnO NPs(SO_4^{2-})) (**b**) after 24 h incubation. Scratch width, mm (median, *p<0.05).

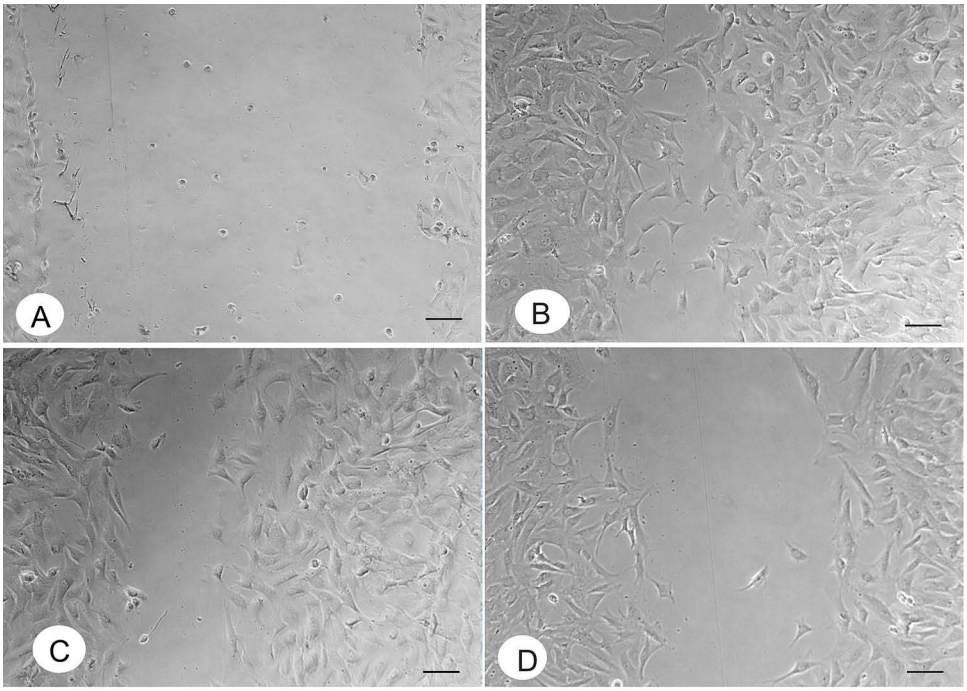

Figure 7 Scratch assay demonstrates that exposure to dextran-polyacrylamide/ZnO NPs from zinc sulphate (D-PAA/ZnO NPs(SO_4^{2-})) reduces the motility of fibroblasts at concentrations 3.07 mM and above in contrast to D-PAA/ZnO NPs(-OAc): a representative control sample directly after scratching, 0 h (**A**); a representative control sample, 24 h (**B**); a representative monolayer exposed to dextran-polyacrylamide/ZnO NPs from zinc acetate (D-PAA/ZnO NPs(-OAc)) at 12.3 mM, 24 h (**C**); a representative monolayer exposed to D-PAA/ZnO NPs(SO_4^{2-}) at 12.3 mM, 24 h (**D**). Scale bar: 100 μm.

NPs(SO_4^{2-}) nanosystem, as supported by DLS and FL data. Furthermore, we did not observe significant cytotoxicity of either type of nanosystem against fibroblasts in vitro.

Previous studies have also investigated the cytotoxicity of zinc oxide nanoparticles on various cell types. For instance, ovarian germ cells were found to be sensitive to 80 nm zinc oxide nanoparticles at a concentration of 30 mg/mL, resulting in increased production of reactive oxygen species and alterations in germ cell markers.[53] On the other hand, subtoxic concentrations of ZnO NPs did not affect cytokine secretion and differentiation of human adipose tissue-derived stromal cells.[54] Toxic effects on isolated mice bone marrow mesenchymal stem cells were observed with ZnO NPs of 6–8 nm in size, leading to mitochondrial and cytoskeletal disturbances and increased ROS generation at concentrations above 20 mg/mL.[55]

The cytotoxicity of ZnO NPs is known to be dependent on their size. Murine fibroblasts exhibit higher sensitivity to 20 nm nanoparticles compared to those of 40 nm and 80 nm, with toxicity observed at 0.1 mM for 20 nm NPs and 1 mM for 40 nm and 80 nm NPs, respectively.[56] It should be noted that the ZnO NPs used in our study, incorporated within the D-PAA nanosystems, were significantly smaller in size and exhibited lower cytotoxicity towards fibroblasts. This may be attributed to the role of the carrier polymer in facilitating cell penetration, stabilizing the nanoparticles, and preventing their direct interaction with intracellular targets. Additionally, the cytotoxicity is likely mediated by the release of Zn^{2+} ions from the zinc oxide nanoparticles through chemical reactions triggered by pH decrease.[10] Normal cells typically maintain tight control over intracellular pH and homeostasis, which may explain the reduced cytotoxicity of the nanosystems towards normal cells.

Zinc concentration in prostate cancer cells is approximately decreased at 10–25%.[57] Zinc contain in prostate cancer cells was significantly lower than in benign tumors and normal prostates.[58] Breast cancer cells, on the contrary, tend to accumulate zinc.[59] The mechanisms of this phenomenon have not been fully elucidated. Nevertheless, zinc content is a marker of the prostate and breast cancer. Thus, cell lines with different physiological features of regulation of zinc concentration were used.

Previous studies have shown the lack of cytotoxicity of D-PAA polymers against various cell lines.[60–62] The sensitivity of prostate and breast cancer cells to D-PAA/ZnO NPs solutions was determined. Three distinct prostate cancer cell lines with varying degrees of malignancy were used. LNCaP, DU-145 and PC-3 were low, intermediate and high degree of malignancy, respectively. MDA-MB-231 and MCF-7 were breast cancer cells lines. The sensitivity of cancer cells to the influence of different D-PAA/ZnO NPs concentrations was determined. The values of EC50 were calculated. The lowest sensitivity of LNCaP cells to the ZnO NPs influence was revealed. EC50 of ZnO NPs for LNCaP was 2.81±0.14 mM, DU-145 – 2.69±0.15 mM, PC-3 – 2.34±0.2 mM. Thus, with increasing malignancy of cells, their sensitivity to the nanocomposite increases. The sensitivity of breast cancer cells to D-PAA/ZnO NPs was slightly higher. EC50 for MDA-MB-231 was 2.2±0.17 mM, and MCF-7 – 2.21±0.14 mM. The D-PAA/ZnO NPs(-OAc) antitumor activity was lower compared to D-PAA/ZnO NPs(SO_4^{2-}). Antitumor efficiencies of these ZnO NPs are shown in Figure 8.

The maximum effect of ZnO NPs strongly depends on the cell type. The cell death rate was 80% for cells with low and intermediate degrees of malignancy, and 50–60% for cells with high degrees of malignancy. The EC50 for D-PAA/ZnO NPs(-OAc) increased approximately 10-fold to 18–25 mM (Table 1).

It is hypothesized that the cytotoxicity of the nanosystems was primarily caused by non-selective mechanisms, which involve the release and accumulation of Zn^{2+} ions. The D-PAA/ZnO NPs have a large surface area relative to their small dimensions, attributed to the small size of the ZnO NPs (approximately 1–2 nm in radius) and their stabilization in the D-PAA polymer matrix, which prevents aggregation. It results in the rapid accumulation of critical concentrations of Zn^{2+} ions in the cells, aided by the decrease of environmental pH and high lysosomal activity in the cancer cell.[63,64]

The nanosystems exhibited higher cytotoxicity against cancer cells in vitro compared to normal cells. Extensive evidence suggests that nanoparticles (NPs) enter normal and cancer cells at different rates and accumulate in the cytoplasm.[65] The physiological characteristics of cancer cells contribute to increased plasma membrane permeability for various compounds, which is necessary to sustain high levels of cancer cell metabolism. We assume that differences in ZnO NPs cytotoxicity was determined by the metabolic activity of the cells. Similar studies have demonstrated selective apoptosis inhibition in A549 lung cancer cells and reduced migration potential. HaCaT keratinocytes, on the other hand, showed less toxicity from ZnO NPs at concentrations up to 20 mg/L.[66]

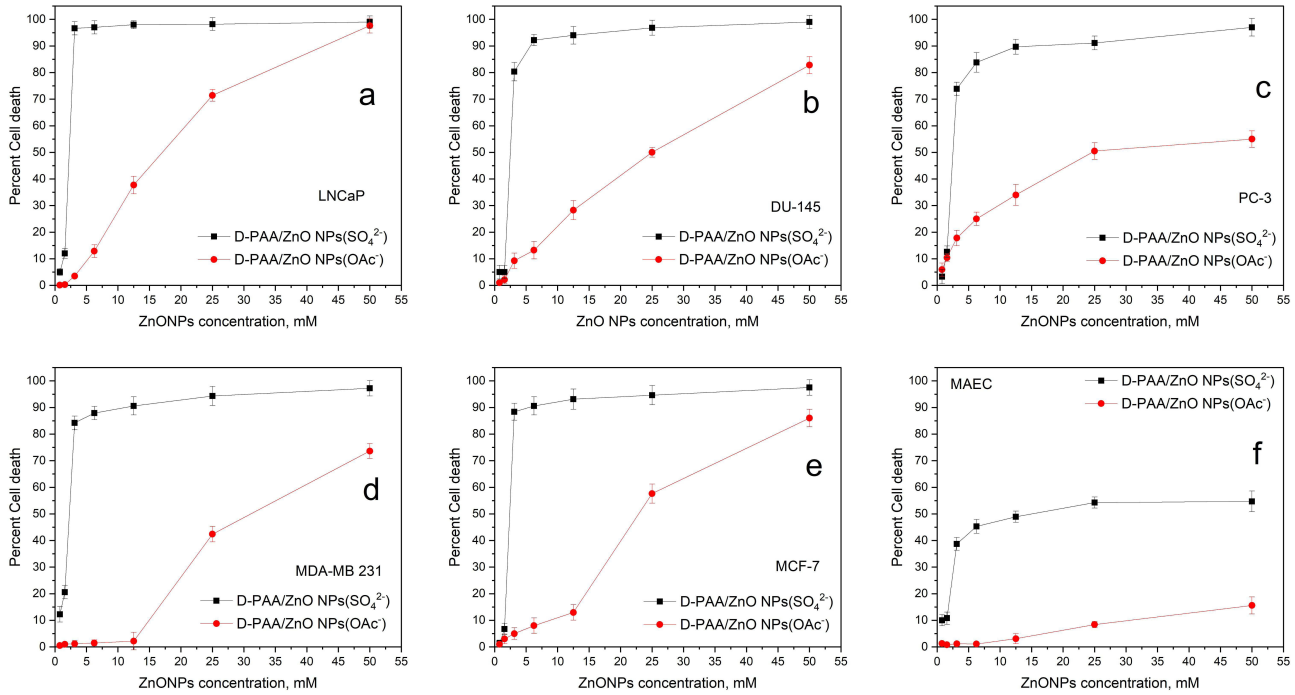

Figure 8 Survival of prostate cancer cell lines LNCaP (**a**), DU-145 (**b**), PC-3 (**c**), breast cancer MDA-MB-231 (**d**), MCF-7 (**e**) and normal cells MAEC (**f**) treated with dextran-polyacrylamide/ZnO NPs from zinc acetate (D-PAA/ZnO NPs(-OAc)) and zinc sulphate (D-PAA/ZnO NPs(SO_4^{2-})) (M±SD).

Table 1 EC50 and Maximal Percentage of Cell Death in Prostate Cancer Cell Lines, Breast Cancer Cells, and Normal Cells Treated with Dextran-Polyacrylamide/ZnO NPs Derived from Zinc Acetate (D-PAA/ZnO NPs(-OAc)) and Zinc Sulfate (D-PAA/ZnO NPs(SO_4^{2-})) (Mean ± SD)

Cells Line	EC50 (mM)		Maximal Percent Cell Death (for 50 mM [Zn])	
	D-PAA/ZnO NPs (SO_4^{2-})	D-PAA/ZnO NPs (-OAc)	D-PAA/ZnO NPs (SO_4^{2-})	D-PAA/ZnO NPs (-OAc)
LNCaP	2.81±0.14	17.3±0.14	99.0±2.3	97.6±2.8
DU-145	2.69±0.15	25.0±0.24[a]	99.0±2.5	82.8±3.2
PC-3	2.34±0.2	–[b]	97.0±3.3	55.0±3.1
MDA-MB-231	2.2±0.17	–[b]	97.2±2.9	73.6±2.8
MCF-7	2.21±0.14	23.2±0.22[a]	97.5±2.9	86.0±3.3
MAEC	–[b]	–[b]	54.7±3.9	15.6±3.2

Notes: Prostate cancer cells line were LNCaP, DU-145, PC-3, breast cancer cells were MDA-MB-231, MCF-7, normal cells were MAEC. [a]EC50 is approximate due to lack of close to 100% cell death; [b]EC50 can not be calculated.

The selective cytotoxicity of ZnO NPs on co-cultured C2C12 myoblastoma cells and 3T3-L1 adipocytes has been described. Increased expression of proapoptotic proteins was observed in both cell types, but 3T3-L1 adipocytes exhibited significantly lower sensitivity to ZnO NPs.[67] Co-crystallized zinc oxide with tea polyphenol and epigallocatechin-3-gallate has been shown to induce cell death in PC-3 prostate cancer cells while remaining non-toxic to WI-38 lung fibroblasts.[68]

A high concentration of zinc can lead to protein denaturation.[69,70] In response to this, cells undergo a series of adaptive changes to repair the damage. However, if the damage is severe and cannot be repaired, the cells initiate apoptosis. Some intracellular proteins may become unfolded or misfolded, forming protein aggregates. If the ubiquitin-dependent systems fail to repair the damage, apoptosis is triggered.[71]

In our previous studies, we analyzed expression changes of apoptosis and proliferation-associated markers, namely p53, Ki-67, Bcl-2, and Bax, in prostate cancer cell lines LNCaP, DU-145, and PC-3.[72] Upregulation of the pro-apoptotic proteins p53 and Bax was demonstrated, while Bcl-2 and Ki-67 showed simultaneous downregulation. Similar results were observed in breast cancer cells (Figure 9). After incubation with D-PAA/ZnO NPs, the expression of p53 increased

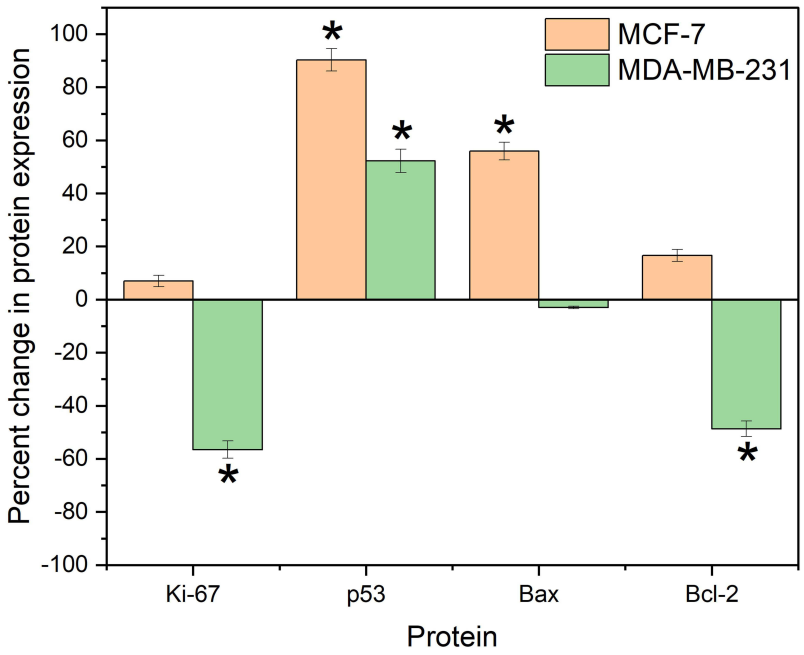

Figure 9 Expression of Ki-67, p53, Bax and Bcl-2 in breast cancer cells lines MDA-MB-231, MCF-7 treated with dextran-polyacrylamide/ZnO NPs from zinc sulphate (D-PAA/ZnO NPs(SO_4^{2-})). Line "0" is basic protein expression. (M±SD, *p<0.05).

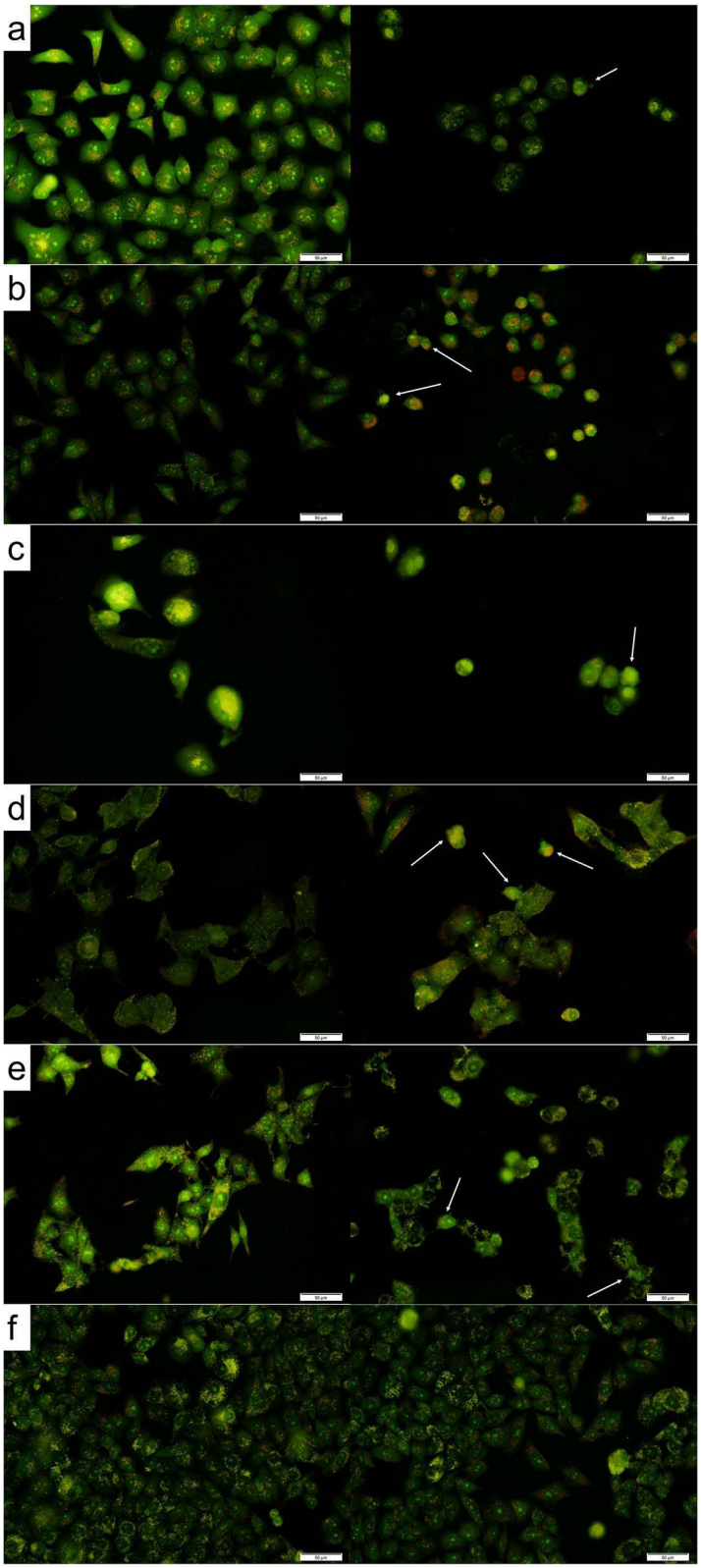

Figure 10 Changing of morphology of prostate cancer cell lines LNCaP (**a**), DU-145 (**b**), PC-3 (**c**), breast cancer MDA-MB-231 (**d**), MCF-7 (**e**) and normal cells MAEC (**f**) treated with dextran-polyacrylamide/ZnO NPs from zinc sulphate (D-PAA/ZnO NPs(SO_4^{2-})). Right – control, left - incubation with EC50 D-PAA/ZnO NPs(SO_4^{2-}) for 24 hours. (MAEC was incubated at 3 mM D-PAA/ZnO NPs(SO_4^{2-}) that more then EC50 for cancer cells; staining with acridine Orange 0.002 mg/mL in saline for 1 min; arrows show cells in the last stages of apoptosis).

10-fold in MCF-7 cells and 2-fold in MDA-MB-231 cells. Additionally, the levels of Ki-67 and Bcl-2 were decreased in MDA-MB-237 cells. However, no statistically significant expression changes of these proteins were found in MCF-7 cells. We think that the differential response to D-PAA/ZnO NPs is influenced by the physiological characteristics of different cancer cell lines.

Morphological changes in cells were evaluated after 24 hours of incubation with D-PAA/ZnO NPs(SO_4^{2-}), which was chosen for its higher cancer toxicity compared to D-PAA/ZnO NPs(-OAc). Figure 10 shows fluorescent images of cancer cells stained with acridine orange. Control samples exhibited single spherical cells with no noticeable changes in nucleus and cytoplasm size. However, incubation with D-PAA/ZnO NPs(SO_4^{2-}) resulted in a significant increase of the spherical cells number, where the nucleus occupied almost the entire cell. Cells in advanced stages of apoptosis with the formation of apoptotic bodies were detected in all investigated cancer cell lines after the addition of D-PAA/ZnO NPs(SO_4^{2-}) (Figure 10, indicated by arrows).

Thus, the nanocomposite promotes apoptosis in prostate and breast cancer cells. However, other regulated cell death modalities such as autophagy, necrosis, or ferroptosis cannot be excluded, given the significant regulatory role of ROS signaling in these cell death modes. A decrease of adhesion of MDA-MB-231 cells to the surface during incubation with nanocomposites was observed. The expression of E-cadherin, N-cadherin, and CD44 was investigated. MDA-MB-231 showed a 45% decrease of expression of E- and N-cadherins (Figure 11b).

In other cancer cell lines, the expression of these proteins increased to varying degrees. E-cadherin and N-cadherin play important roles in intercellular adhesion as well as they are factors in contact inhibition of proliferation and metastasis in advanced stages of cancer.[73,74] The functions of CD44 in cancer progression are controversial, as the protein has many isoforms that serve as markers of oncological cell transformation.[75] No statistically significant changes of CD44 expression were detected in LNCaP and MDA-MB-231 cells, while it increased by 39.6% for PC-3 and decreased by 50.9% for DU-145 and 32.4% for MCF-7 (Figure 11a and b). In general, it can be concluded that D-PAA/ZnO NPs(SO_4^{2-}) induce apoptosis and increase the expression of adhesion proteins. This may potentially reduce the ability of tumors to metastasize and aid in their treatment. However, the data for MDA-MB-231 cells show the opposite reaction with decreased adhesion. Therefore, further research is needed to elucidate the mechanism of action of D-PAA/ZnO NPs(SO_4^{2-}) on different types of cancer cells.

It should be noted, D-PAA/ZnO NPs obtained from $ZnSO_4$ are able to effectively eliminate various types of cancer cells in vitro. In the future, it is necessary to determine the interaction mechanisms of these nanocomposites with normal and cancer cells as well as their ability to targeted delivery of active components to tumors without influence on normal tissues.

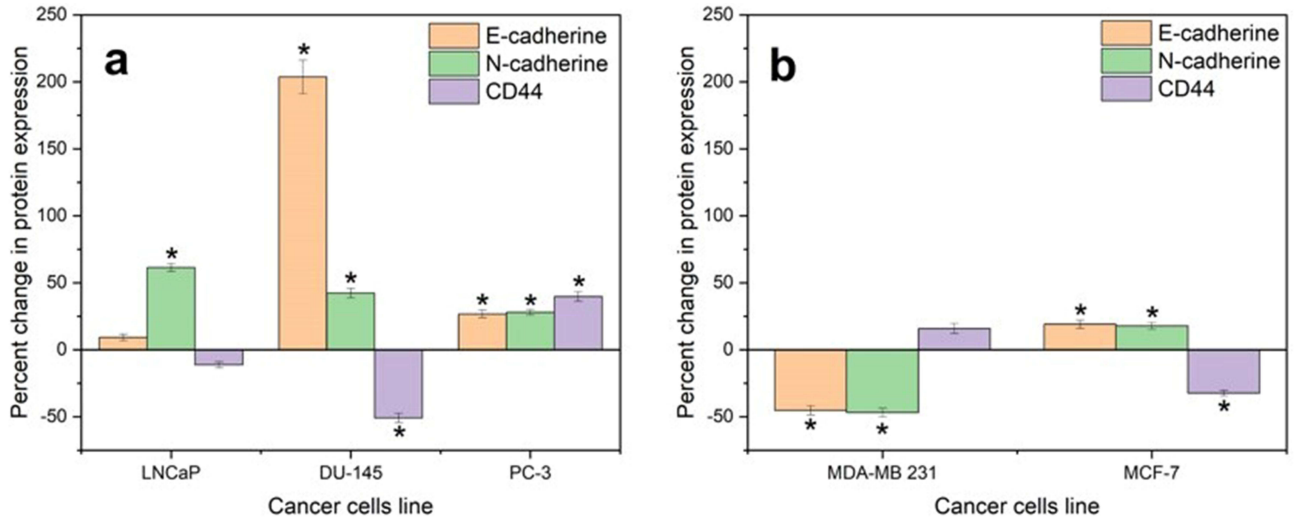

Figure 11 Expression of E-cadherin, N-cadherin and CD44 in prostate cancer cell lines (**a**) LNCaP, DU-145, PC-3 and breast cancer (**b**) MDA-MB-231, MCF-7 treated with dextran-polyacrylamide/ZnO NPs from zinc sulphate (D-PAA/ZnO NPs(SO_4^{2-})). Line "0" is basic protein expression. (M±SD, *p<0.05).

Conclusion

Two hybrid nanosystems, D-PAA/ZnO NPs(SO_4^{2-}) and D-PAA/ZnO NPs(-OAc), were synthesized using zinc sulphate and zinc acetate as precursors, respectively. These nanosystems consist of zinc oxide nanoparticles (ZnO NPs) as the cytotoxic agent and dextran-graft-polyacrylamide copolymer (D-PAA) as the nanocarrier. The radius of the ZnO NPs was 1–2 nm, which is much smaller than those obtained through green synthesis, sol-gel, and co-precipitation methods (which typically have radii ranging from 15 to 50 nm). The D-PAA copolymer effectively stabilized the ZnO NPs, resulting in small-sized nanoparticles (not exceeding 40 nm) and a low number of aggregates.

Both D-PAA/ZnO NPs(SO_4^{2-}) and D-PAA/ZnO NPs(-OAc) demonstrated low toxicity to fibroblasts and MAEC cells. However, the D-PAA/ZnO NPs nanosystem synthesized using zinc sulphate exhibited higher anticancer activity compared to the sample prepared using zinc acetate. These nanosystems effectively destroyed prostate cancer cell lines (LNCaP, PC-3, DU-145) and breast cancer cell lines (MDA-MB-231, MCF-7) in vitro, primarily through apoptosis. An expression increase of proapoptotic proteins and corresponding morphological changes in the cells were observed. The increased expression of E-cadherin and N-cadherin suggests about decrease of the metastatic potential of the cells.

These findings indicate the selective cytotoxicity of D-PAA/ZnO NPs against cancer cells and suggest their potential use in cancer treatment. The observed difference in anticancer activity between D-PAA/ZnO NPs(SO_4^{2-}) and D-PAA/ZnO NPs(-OAc) nanosystems is likely attributed to differences in nanoparticle size, as well as differences in their permeability and interaction with cells. However, further research is required to explore these assumptions and to elucidate the mechanism of action of D-PAA/ZnO NPs nanosystems on different cell types.

Acknowledgments

The authors thank to University of Strasbourg-Institut Charles Sadron (Strasbourg, France), French PAUSE program for emergency welcome of Ukrainian scientist Dr. Nataliya Kutsevol (2022–2023), Catherine Foussat and Mélanie Legros from the characterization group of the Institut Charles Sadron for size exclusion chromatography for polymer. Authors are grateful to brave defenders of Ukraine for the opportunity to finalize this publication.

Funding

This study was supported in part by the Ministry of the Education and Science of Ukraine, Project no. 0122U001818 and by National Research Foundation of Ukraine Project 2020.02/0022, Research program of the NAS of Ukraine (No. 0118U005468), Guangxi Innovation Driven Development Major Project (No. Guike AA20302013), Nanning Scientific Research and Technology Development Plan Project (No. RC20200001), Yongjiang Plan Project of Leading Talents of Innovation and Entrepreneurship in Nanning City (No. 2020024), Yulin City Science and Technology Transformation Project (No. 19040003).

Disclosure

The authors report no conflicts of interest in this work.

References

1. Damodharan J. Nanomaterials in medicine – an overview. *Mater Today Proc*. 2021;37:383–385.
2. Lan J, Teekaraman Y. Overview of application of nanomaterials in medical domain. *Contrast Media Mol Imaging*. 2022;2022:3507383. doi:10.1155/2022/3507383
3. Guo D, Wu C, Jiang H, et al. Synergistic cytotoxic effect of different sized ZnO nanoparticles and daunorubicin against leukemia cancer cells under UV irradiation. *J Photochem Photobiol B*. 2008;93(3):119–126. doi:10.1016/j.jphotobiol.2008.07.009
4. Nair S, Sasidharan A, Divya Rani VV, et al. Role of size scale of ZnO nanoparticles and microparticles on toxicity toward bacteria and osteoblast cancer cells. *J Mater Sci Mater Med*. 2009;20(S1):235–241. doi:10.1007/s10856-008-3548-5
5. Cheng Z, M. L, Dey R, et al. Nanomaterials for cancer therapy: current progress and perspectives. *J Hematol Oncol*. 2021;14:85. doi:10.1186/s13045-021-01096-0
6. Skrajnowska D, Bobrowska-Korczak B. Role of zinc in immune system and anti-cancer defense mechanisms. *Nutrients*. 2019;11(10):2273. doi:10.3390/nu11102273
7. John E, Laskow TC, Buchser WJ, et al. Zinc in innate and adaptive tumor immunity. *J Transl Med*. 2010;8(1):118. doi:10.1186/1479-5876-8-118
8. Kavousi Heidari M, Pourmadadi M, Yazdian F, et al. Wound dressing based on PVA nanofiber containing silk fibroin modified with GO/ZnO nanoparticles for superficial wound healing: in vitro and in vivo evaluations. *Biotechnol Prog*. 2023;39:e3331. doi:10.1002/btpr.3331

9. Rasmussen JW, Martinez E, Louka P, et al. Zinc oxide nanoparticles for selective destruction of tumor cells and potential for drug delivery applications. *Expert Opin Drug Deliv*. 2010;7(9):1063–1077. doi:10.1517/17425247.2010.502560
10. Singh TA, Das J, Sil PC. Zinc oxide nanoparticles: a comprehensive review on its synthesis, anticancer and drug delivery applications as well as health risks. *Adv Colloid Interface Sci*. 2020;286:102317. doi:10.1016/j.cis.2020.102317
11. Yazdian F. Aptamer-functionalized quantum dots for targeted cancer therapy. In: Kesharwani P, editor. *Book: Aptamers Engineered Nanocarriers for Cancer Therapy*. Woodhead Publishing Series in Biomaterials; 2023:295–315.
12. Ohgaki M, Kizuki T, Katsura M, et al. Manipulation of selective cell adhesion and growth by surface charges of electrically polarized hydroxyapatite. *J Biomed Mater Res*. 2001;57(3):366–373. doi:10.1002/1097-4636(20011205)57:3<366::AID-JBM1179>3.0.CO;2-X
13. Jiang J, Pi J, Cai J. The advancing of zinc oxide nanoparticles for biomedical applications. *Bioinorg Chem Appl*. 2018;2018:1062562. doi:10.1155/2018/1062562
14. Hanley C, Layne J, Punnoose A, et al. Preferential killing of cancer cells and activated human T cells using zinc oxide nanoparticles. *Nanotechnology*. 2008;19:295103–295113. doi:10.1088/0957-4484/19/29/295103
15. Hanley C, Thurber A, Hanna C, et al. The influences of cell type and ZnO nanoparticle size and immune cell cytotoxicity and cytokine induction. *Nanoscale Res Lett*. 2009;4(12):1409–1420. doi:10.1007/s11671-009-9413-8
16. Ward C, Meehan J, Gray ME, et al. The impact of tumour pH on cancer progression: strategies for clinical intervention. *Explor Target Antitumor Ther*. 2020;1:71–100. doi:10.37349/etat.2020.00005
17. Reed RB, Ladner DA, Higgins CP, Westerhoff P, Ranville JF. Solubility of nano-zinc oxide in environmentally and biologically important matrices. *Environ Toxicol Chem*. 2012;31(1):93–99. doi:10.1002/etc.708
18. Unsoy G, Gunduz U. Smart drug delivery systems in cancer therapy. *Curr Drug Targets*. 2018;19(3):202–212. doi:10.2174/1389450117666160401124624
19. Edis Z, Wang J, Waqas MK, et al. Nanocarriers-mediated drug delivery systems for anticancer agents: an overview and perspectives. *Int J Nanomedicine*. 2021;16:1313–1330. doi:10.2147/IJN.S289443
20. Senapati S, Mahanta A, Kumar S, et al. Controlled drug delivery vehicles for cancer treatment and their performance. *Signal Transduct Target Ther*. 2018;3(1):7. doi:10.1038/s41392-017-0004-3
21. Anjum S, Hashim M, Malik SA, et al. Recent advances in Zinc Oxide Nanoparticles (ZnO NPs) for cancer diagnosis, target drug delivery, and treatment. *Cancers*. 2021;13(18):4570. doi:10.3390/cancers13184570
22. Scherzad A, Meyer T, Kleinsasser N, et al. Molecular mechanisms of zinc oxide nanoparticle-induced genotoxicity short running title: genotoxicity of ZnO NPs. *Materials*. 2017;10(12):1427. doi:10.3390/ma10121427
23. Mawed SA, Marini C, Alagawany M, et al. Zinc Oxide Nanoparticles (ZnO-NPs) suppress fertility by activating autophagy, apoptosis, and oxidative stress in the developing oocytes of female Zebrafish. *Antioxidants*. 2022;11(8):1567. doi:10.3390/antiox11081567
24. Patra JK, Das G, Fraceto LF, et al. Nano based drug delivery systems: recent developments and future prospects. *J Nanobiotechnology*. 2018;16(1):71. doi:10.1186/s12951-018-0392-8
25. Di Veroli G, Fornari C, Goldlust I, et al. An automated fitting procedure and software for dose-response curves with multiphasic features. *Sci Rep*. 2015;5(1):14701. doi:10.1038/srep14701
26. Chang Y, Guo K, Li Q, et al. Multiple directional differentiation difference of neonatal rat fibroblasts from six organs. *Cell Physiol Biochem*. 2016;39(1):157–171. doi:10.1159/000445613
27. Kutsevol N, Glamazda A, Chumachenko V, et al. Behavior of hybrid thermosensitive nanosystem dextran-graft-pnipam/gold nanoparticles: characterization within LCTS. *J Nanopart Res*. 2018;20(9):236. doi:10.1007/s11051-018-4331-2
28. Bulavin L, Kutsevol N, Chumachenko V, et al. SAXS combined with UV-vis spectroscopy and QELS: accurate characterization of silver sols synthesized in polymer matrices. *Nanoscale Res Lett*. 2016;11(1):35. doi:10.1186/s11671-016-1230-2
29. Avramović N, Mandić B, Savić-Radojević A, et al. Polymeric nanocarriers of drug delivery systems in cancer therapy. *Pharmaceutics*. 2020;12(4):298. doi:10.3390/pharmaceutics12040298
30. Chumachenko VA, Shton IO, Shishko ED, et al. Branched copolymers dextran-graft-polyacrylamide as nanocarriers for delivery of gold nanoparticles and photosensitizers to tumor cells. In: Fesenko O, Yatsenko L, editors. *Book: Nanophysics, Nanophotonics, Surface Studies, and Applications, Springer Proceedings in Physics.* Vol. 183. Cham, Switzerland: Springer; 2016:379–390.
31. Grebinyk A, Prylutska S, Grebinyk S, et al. Drug delivery with pH-sensitive star-like dextran - graft polyacrylamide copolymer. *Nanoscale adv*. 2022;4(23):5077–5088. doi:10.1039/D2NA00353H
32. Lim E-K, Chung BH, Chung SJ. Recent advances in pH-sensitive polymeric nanoparticles for smart drug delivery in cancer therapy. *Curr Drug Targets*. 2018;19(4):300–317. doi:10.2174/1389450117666160602202339
33. Kutsevol N, Bezugla T, Bezuglyi M, et al. Branched dextran- graft -polyacrylamide copolymers as perspective materials for nanotechnology. *Macromol Symp*. 2012;317–318(1):82–90. doi:10.1002/masy.201100087
34. Hulkower KI, Herber RL. Cell migration and invasion assays as tools for drug discovery. *Pharmaceutics*. 2011;3(1):107–124. doi:10.3390/pharmaceutics3010107
35. McClelland RA, Wilson D, Leake R, et al. A multicentre study into the reliability of steroid receptor immunocytochemical assay quantification. British Quality Control Group. *Eur J Cancer*. 1991;27(6):711–715. doi:10.1016/0277-5379(91)90171-9
36. Goldburg WI. Dynamic light scattering. *Am J Phys*. 1999;67(12):1152–1160. doi:10.1119/1.19101
37. Berne BJ, Pecora R. *Dynamic Light Scattering: With Applications to Chemistry, Biology, and Physics*. Mineola: Courier Dover Publications; 2000.
38. Aldalbahi A, Alterary S, Ali Abdullrahman Almoghim R, et al. Greener synthesis of zinc oxide nanoparticles: characterization and multifaceted applications. *Molecules*. 2020;25(18):4198. doi:10.3390/molecules25184198
39. Iqbal J, Abbasi BA, Yaseen T, et al. Green synthesis of zinc oxide nanoparticles using Elaeagnus angustifolia L. leaf extracts and their multiple in vitro biological applications. *Sci Rep*. 2021;11(1):20988. doi:10.1038/s41598-021-99839-z
40. Alhoqail WA, Alothaim AS, Suhail M, et al. Husk-like zinc oxide nanoparticles induce apoptosis through ROS generation in epidermoid carcinoma cells: effect of incubation period on sol-gel synthesis and anti-cancerous properties. *Biomedicines*. 2023;11(2):320. doi:10.3390/biomedicines11020320
41. Balcha A, Yadav OP, Dey T. Photocatalytic degradation of methylene blue dye by zinc oxide nanoparticles obtained from precipitation and sol-gel methods. *Environ Sci Pollut Res Int*. 2016;23(24):25485–25493. doi:10.1007/s11356-016-7750-6
42. Zahra S, Bukhari H, Qaisar S, Sheikh A, Amin A. Synthesis of nanosize zinc oxide through aqueous sol-gel route in polyol medium. *BMC Chem*. 2022;16(1):104. doi:10.1186/s13065-022-00900-3

43. Katiyar A, Kumar N, Shukla RK, Srivastava A. Influence of alkali hydroxides on synthesis, physico-chemical and photoluminescence properties of zinc oxide nanoparticles. *Mater Today Proc*. 2020;29:885–889.
44. Adam RE, Pozina G, Willander M, Nur O. Synthesis of ZnO nanoparticles by co-precipitation method for solar driven photodegradation of Congo red dye at different pH. *Photonics Nanostruct*. 2018;32:11–18. doi:10.1016/j.photonics.2018.08.005
45. Reynolds DC, Look DC, Jogai B, et al. Neutral-donor-bound-exciton complexes in ZnO crystals. *Phys Rev B*. 1998;57:12151. doi:10.1103/PhysRevB.57.12151
46. Viswanatha R, Sapra S, Satpati B, et al. Understanding the quantum size effects in ZnO nanocrystals. *J Mater Chem*. 2004;14(4):661–668. doi:10.1039/b310404d
47. Song Z, Kelf TA, Washington H, et al. Characterization of optical properties of ZnO nanoparticles for quantitative imaging of transdermal transport. *Biomed Opt Express*. 2011;2:3321–3333. doi:10.1364/BOE.2.003321
48. Akhtar MJ, Ahamed M, Kumar S, et al. Zinc oxide nanoparticles selectively induce apoptosis in human cancer cells through reactive oxygen species. *Int J Nanomedicine*. 2012;7:845–857. doi:10.2147/IJN.S29129
49. Taccola L, Raffa V, Riggio C, et al. Zinc oxide nanoparticles as selective killers of proliferating cells. *Int J Nanomedicine*. 2011;6:1129–1140. doi:10.2147/IJN.S16581
50. Vinardell MP, Mitjans M. Antitumor activities of metal oxide nanoparticles. *Nanomaterials*. 2015;5:1004–1021. doi:10.3390/nano5021004
51. Guo D, Bi H, Liu B, et al. Reactive oxygen species-induced cytotoxic effects of zinc oxide nanoparticles in rat retinal ganglion cells. *Toxicol In Vitro*. 2013;27(2):731–738. doi:10.1016/j.tiv.2012.12.001
52. Yang D, Zhang M, Gan Y, et al. Involvement of oxidative stress in ZnO NPs-induced apoptosis and autophagy of mouse GC-1 spg cells. *Ecotoxicol Environ Saf*. 2020;202:110960. doi:10.1016/j.ecoenv.2020.110960
53. Saber M, Hayaei-Tehrani RS, Mokhtari S, et al. In vitro cytotoxicity of zinc oxide nanoparticles in mouse ovarian germ cells. *Toxicol In Vitro*. 2021;70:105032. doi:10.1016/j.tiv.2020.105032
54. Radeloff K, Radeloff A, Tirado MR, et al. Long-term impact of zinc oxide nanoparticles on differentiation and cytokine secretion of human adipose-derived stromal cells. *Materials*. 2019;12(11):1823. doi:10.3390/ma12111823
55. Syama S, Sreekanth PJ, Varma HK, Mohanan PV. Zinc oxide nanoparticles induced oxidative stress in mouse bone marrow mesenchymal stem cells. *Toxicol Mech Methods*. 2014;24(9):644–653. doi:10.3109/15376516.2014.956914
56. Sirelkhatim A, Mahmud S, Seeni A, et al. Preferential cytotoxicity of ZnO nanoparticle towards cervical cancer cells induced by ROS-mediated apoptosis and cell cycle arrest for cancer therapy. *J Nanopart Res*. 2016;18(8):219. doi:10.1007/s11051-016-3531-x
57. Costello LC, Franklin RB. The clinical relevance of the metabolism of prostate cancer; zinc and tumor suppression: connecting the dots. *Mol Cancer*. 2006;5(1):17. doi:10.1186/1476-4598-5-17
58. Zhao J, Wu Q, Hu X, et al. Comparative study of serum zinc concentrations in benign and malignant prostate disease: a systematic review and meta-analysis. *Sci Rep*. 2016;6(1):25778. doi:10.1038/srep25778
59. Cui Y, Vogt S, Olson N, et al. Levels of zinc, selenium, calcium, and iron in benign breast tissue and risk of subsequent breast cancer. *Cancer Epidemiol Biomarkers Prev*. 2007;16(8):1682–1685. doi:10.1158/1055-9965.EPI-07-0187
60. Yurchenko A, Nikitina N, Sokolova V, et al. Novel branched copolymer-containing anticancer drug for targeted therapy: in vitro research. *BioNanoSci*. 2020;10:249–259. doi:10.1007/s12668-019-00700-5
61. Kutsevol N, Kuziv Y, Bezugla T, et al. Multicomponent nanocomposites for complex anticancer therapy: effect of aggregation processes on their efficacy. *Int J Pol Sci*. 2020;2020:9627954.
62. Telegeev G, Kutsevol N, Chumachenko V, et al. Dextran-polyacrylamide as matrices for creation of anticancer nanocomposite. *Int J Pol Sci*. 2017;2017:4929857.
63. Boedtkjer E, Pedersen SF. The acidic tumor microenvironment as a driver of cancer. *Annu Rev Physiol*. 2020;82(1):103–126. doi:10.1146/annurev-physiol-021119-034627
64. Tang T, Yang Z, Wang D, et al. The role of lysosomes in cancer development and progression. *Cell Biosci*. 2020;10:131. doi:10.1186/s13578-020-00489-x
65. Ibraheem S, Kadhim AA, Kadhim KA, et al. Zinc oxide nanoparticles as diagnostic tool for cancer cells. *Int J Biomater*. 2022;2022:2807644. doi:10.1155/2022/2807644
66. Jin Y, Rupa EJ, Nahar J, et al. Hydroponic ginseng ROOT mediated with CMC polymer-coated zinc oxide nanoparticles for cellular apoptosis via downregulation of BCL-2 gene expression in A549 lung cancer cell line. *Molecules*. 2023;28(2):906. doi:10.3390/molecules28020906
67. Chandrasekaran M, Pandurangan M. In vitro selective anti-proliferative effect of zinc oxide nanoparticles against co-cultured C2C12 myoblastoma cancer and 3T3-L1 normal cells. *Biol Trace Elem Res*. 2016;172:148–154. doi:10.1007/s12011-015-0562-6
68. Samutprasert P, Chiablaem K, Teeraseranee C, et al. Epigallocatechin gallate-zinc oxide co-crystalline nanoparticles as an anticancer drug that is non-toxic to normal cells. *RSC Adv*. 2018;8(14):7369–7376. doi:10.1039/C7RA10997K
69. Hu JY, Zhang DL, Liu XL, et al. Pathological concentration of zinc dramatically accelerates abnormal aggregation of full-length human Tau and thereby significantly increases Tau toxicity in neuronal cells. *Biochim Biophys Acta Mol Basis Dis*. 2017;1863(2):414–427. doi:10.1016/j.bbadis.2016.11.022
70. Ramirez-Bello V, Martinez-Seoane J, Fernández-Silva A, Amero C. Zinc and copper ions induce aggregation of human β-crystallins. *Molecules*. 2022;27(9):2970. doi:10.3390/molecules27092970
71. Li Y, Li S, Wu H. Ubiquitination-Proteasome System (UPS) and autophagy two main protein degradation machineries in response to cell stress. *Cells*. 2022;11(5):851. doi:10.3390/cells11050851
72. Virych PA, Zadvorniy TV, Borikun TV, et al. Effects of dextran-graft-polyacrylamide/ZnO nanoparticles on prostate cancer cell lines in vitro. *Exp Oncol*. 2022;44(3):217–221. doi:10.32471/exp-oncology.2312-8852.vol-44-no-3.18452
73. Mendonsa AM, Na TY, Gumbiner BM. E-cadherin in contact inhibition and cancer. *Oncogene*. 2018;37(35):4769–4780. doi:10.1038/s41388-018-0304-2
74. Cao ZQ, Wang Z, Leng P. Aberrant N-cadherin expression in cancer. *Biomed Pharmacother*. 2019;118:109320. doi:10.1016/j.biopha.2019.109320
75. Hassn Mesrati M, Syafruddin SE, Mohtar MA, et al. CD44: a multifunctional mediator of cancer progression. *Biomolecules*. 2021;11(12):1850. doi:10.3390/biom11121850
76. Damaghi M, Wojtkowiak JW, Gillies RJ. pH sensing and regulation in cancer. *Front Physiol*. 2013;4:370. doi:10.3389/fphys.2013.00370